Cation size control of structure, structural fluctuations, and superconductivity in $L_{1.85}M_{0.15}CuO_4$

Judith A. McAllister and J. Paul Attfield
Department of Chemistry, University of Cambridge, Lensfield Road, Cambridge, CB2 1EW, United Kingdom and the Interdisciplinary Research Centre in Superconductivity, Department of Physics, Madingley Road, Cambridge, CB3 0HE, United Kingdom

(Received 1 February 2001; revised manuscript received 10 August 2001; published 1 July 2002)

The structural effects of changing the cation size variance σ^2 in $L_{1.85}M_{0.15}CuO_4$ superconductors (A site cations: L^{3+}=La, Nd; M^{2+}=Ca, Sr, Ba) have been determined through neutron powder-diffraction studies of two series of samples, each with a fixed average A site radius $\langle r_A\rangle$. The variance couples strongly to the orthorhombic strain leading to a strong linear increase of the $I4/mmm$ to *Abma* symmetry and *Abma* to *Pccn* symmetry structural phase-transition temperatures with σ^2. The latter transition is shown to occur at a critical orthorhombic strain. Both the mean value and the root-mean-square fluctuations of the Cu-O-Cu angle increase linearly with σ^2 and the suppression of the superconducting T_c by the fluctuations is greater than the suppression by the mean angle by a factor of ~2. The results have been used to construct phase diagrams, projected on the chemical window, for the $L_{1.85}M_{0.15}CuO_4$ system that show a large region in which superconductivity is suppressed by formation of the low-temperature tetragonal $P4_2/ncm$ superstructure.

DOI: 10.1103/PhysRevB.66.014514 PACS number(s): 74.72.Dn, 74.62.Dh, 74.25.Dw, 74.62.Bf

INTRODUCTION

The structural phases of the doped La_2CuO_4-type superconductors are important because large variations in property can be induced by varying the A ($=L_{1-x}M_x$; L^{3+}=La, Nd, etc., M^{2+}=Ca, Sr, Ba) site cation mixture even at a constant hole doping level x.[1] Buckling of the copper oxide planes and distortions of the CuO_6 octahedra generally result in a suppression of superconductivity.[2] Four La_2CuO_4-type structures are known. The parent compound, La_2CuO_4, undergoes a transition from the high-temperature tetragonal (HTT, space group $I4/mmm$) to the low-temperature orthorhombic-1 (LTO1, space group *Abma*) structure at 550 K.[3] Further transitions to the low-temperature orthorhombic-2 (LTO2, space group *Pccn*),[4] and the low-temperature tetragonal (LTT, space group $P4_2/ncm$) (Ref. 5) structures can also occur. The LTO2 type has been observed in Nd- and Sm-doped $La_{2-x}Sr_xCuO_4$.[6] The LTT phase has been of particular interest as it is associated with the suppression of superconductivity around $x=\frac{1}{8}$ in $La_{2-x}Ba_xCuO_4$,[7–9] due to the pinning of charge ordered stripes which have been observed in $La_{1.48}Nd_{0.40}Sr_{0.12}CuO_4$.[10]

The above four superstructures were described using the tilts of the CuO_6 octahedra as order parameters.[11] In the HTT structure, which has a tetragonal $a\times a\times c$ unit cell (indicated by $_T$ subscripts), there is no tilting of the octahedra, whereas the LTO1 has tilting about the $[110]_T$ (or $[1\bar{1}0]_T$) axis of the tetragonal parent structure, towards the $[100]_O$ direction in the resulting $\sqrt{2}a\times\sqrt{2}a\times c$ orthorhombic ($_O$ subscripts) supercell. The transitions to LTO2 and LTT symmetries generally occur over a broad (>20 K) interval and the average CuO_6 octahedral tilt direction changes from $[100]_O$ to $[110]_O$. However, several studies using x-ray-absorption fine structure (XAFS),[12,13] electron microscopy,[14,15] and pair distribution function (PDF) analysis of neutron powder-diffraction data[16] have suggested that the octahedra always tilt about $[110]_T$ (or $[\bar{1}10]_T$) and the long-range order observed by diffraction techniques is a coherent average of the local tilts.[17]

Recent studies have shown that the effects of the A cation distribution are described to a good approximation using three variables.[18,19] The doping level x and the mean A cation radius $\langle r_A\rangle$ are well known, to these we add the A cation size variance σ^2 ($=\langle r_A^2\rangle-\langle r_A\rangle^2$). Previous studies of series of polycrystalline $L_{1.85}M_{0.15}CuO_4$ samples in which the average radius ($\langle r_A\rangle$) is held constant have shown that T_c decreases linearly with σ^2.[18,19] Sample diamagnetism and transport properties also show strong correlations with σ^2,[2,19] and it was concluded that the suppression of superconductivity results from an increase in carrier trapping as σ^2 increases. Although the average crystal structure might be assumed to remain constant at constant $\langle r_A\rangle$, an initial diffraction study of one series showed this not to be the case,[19] and the HTT to LTO1 structural transition temperature showed a linear increase with σ^2. Hence it is not clear whether the changes in physical properties with σ^2 result from increasing local structural fluctuations, or from changes in the average structure, or a combination of these effects. We have carried out a detailed powder neutron-diffraction study of two series of samples to resolve this issue and to provide a systematic description of the structural variation in the optimally doped $L_{1.85}M_{0.15}CuO_4$ system.

NEUTRON-DIFFRACTION EXPERIMENTS AND REFINEMENTS

The preparation and physical properties of the two series of polycrystalline $L_{1.85}M_{0.15}CuO_4$ samples with $\langle r_A\rangle$ = 1.223 and 1.232 Å have been given in a previous paper[19,20] and their compositions are presented in Table I. Powder neutron-diffraction data were collected on instruments D20, D1B, and D2B at the Institut Laue-Langevin, Grenoble, France. D20 and D1B are high-flux, medium resolution dif-

TABLE I. *A* site composition, σ^2, sample number, structure type(s) at 5 K, cell parameters, volumes, and orthorhombicity (*o*) for the $\langle r_A \rangle = 1.223$ and 1.232 Å series of $L_{1.85}M_{0.15}CuO_4$ samples.

A site composition	σ^2 (Å^2)	Sample number	Structure type at 5 K	*a* (Å)	*b* (Å)	*c* (Å)	*V* (Å^3)	*o*
$\langle r_A \rangle = 1.223$ Å								
$La_{0.925}Sr_{0.075}$	0.0006	1	LTO1	5.347 49(5)	5.323 94(5)	13.1981(2)	375.75(1)	0.0044
$La_{0.925}Sr_{0.060}Ca_{0.008}Ba_{0.007}$	0.0009	2	LTO1	5.349 10(5)	5.324 04(5)	13.1935(2)	375.74(1)	0.0047
$La_{0.925}Sr_{0.045}Ca_{0.017}Ba_{0.013}$	0.0012	3	LTO1	5.352 83(5)	5.324 48(5)	13.1894(1)	375.91(1)	0.0053
$La_{0.925}Sr_{0.030}Ca_{0.025}Ba_{0.020}$	0.0015	4	LTO1	5.355 85(5)	5.324 92(5)	13.1839(1)	376.00(1)	0.0058
$La_{0.925}Sr_{0.008}Ca_{0.037}Ba_{0.030}$	0.0020	5	LTO1	5.359 63(5)	5.326 08(5)	13.1822(1)	376.30(1)	0.0063
$La_{0.900}Nd_{0.025}Ca_{0.037}Ba_{0.038}$	0.0025	6	LTO1	5.361 54(5)	5.326 17(5)	13.1752(1)	376.24(1)	0.0066
$La_{0.875}Nd_{0.050}Ca_{0.032}Ba_{0.043}$	0.0029	7	82% LTO1	5.363 75(5)	5.326 91(5)	13.1679(2)	376.237(4)	0.0069
			18% LTO2	5.3510(2)	5.3377(2)	13.1740(6)	376.27(2)	0.0025
$La_{0.850}Nd_{0.075}Ca_{0.028}Ba_{0.047}$	0.0033	8	68% LTO2	5.3574(2)	5.3338(1)	13.1630(3)	376.14(2)	0.0044
			32% LTT	5.344 81(8)		13.1654(3)	376.10(2)	0
$\langle r_A \rangle = 1.232$ Å								
$La_{0.925}Sr_{0.019}Ba_{0.056}$	0.0035	*L*1	LTO2	5.349 16(7)	5.342 37(7)	13.2317(2)	378.12(1)	0.0013
$La_{0.921}Nd_{0.004}Sr_{0.018}Ba_{0.057}$	0.0036	*L*2	LTO2	5.348 47(7)	5.341 87(7)	13.2319(2)	378.05(1)	0.0012
$La_{0.906}Nd_{0.019}Sr_{0.013}Ba_{0.062}$	0.0039	*L*3	LTO2	5.349 79(8)	5.343 16(7)	13.2294(2)	378.16(1)	0.0012
$La_{0.888}Nd_{0.037}Sr_{0.007}Ba_{0.068}$	0.0043	*L*4	LTO2	5.350 43(8)	5.343 93(8)	13.2246(2)	378.12(1)	0.0012
$La_{0.868}Nd_{0.058}Ba_{0.075}$	0.0047	*L*5	LTO2	5.351 20(8)	5.344 59(8)	13.2209(2)	378.12(1)	0.0012

fractometers with large area position sensitive detectors and were used for variable temperature studies. Data from D1B were collected in 2 K intervals for 2 min while the samples were warmed from 4 to 300 K, in the range $20 \leqslant 2\theta \leqslant 100°$ with 0.2° steps, at a neutron wavelength of 2.52 Å. Data from D20 were collected for $0 \leqslant 2\theta \leqslant 160°$, with $\lambda = 2.41$ Å and between 4 and 300 K in 1 K intervals for 1 min per pattern. The D1B data were analyzed in sequence using the FULLPROF program[21] to fit an orthorhombic structural model at each temperature and the D20 data were fitted in the same way using GSAS.[22] These instruments do not have sufficient resolution to resolve the orthorhombically split peaks in the LTO1 and LTO2 phases so that the refined cell parameters correlate with parameters that describe the peak width. The absolute accuracy of the cell constants and derived quantities such as the orthorhombicity (orthorhombic strain), $o = 2(b-a)/(b+a)$, are therefore low. However, Rietveld fitting the profiles over a range of temperatures using a constant peak shape function gives cell parameters with a high relative accuracy that can be used to determine the temperatures of the structural phase transitions, and to compare different samples studied under identical conditions on the same diffractometer.

The refined cell parameters were used to construct plots of orthorhombicity from which the structural transition temperatures were determined. The plots for each series are presented in Fig. 1. All of the samples show an HTT to LTO1 transition above 180 K and a further transition to LTO2 and LTT superstructures was observed for some samples at lower temperatures. The σ^2 variations of the structural transition temperatures are shown in Fig. 2. The assignments of the low-temperature phases (described below) were made using the highly resolved 5 K D2B data which also give accurate absolute values for the cell constants.

High-resolution powder neutron-diffraction profiles of all the samples were collected at 5 K using instrument D2B. Data were collected for $0 \leqslant 2\theta \leqslant 160°$ in 0.05° steps at a 1.594 Å wavelength in a total collection time of 5 h for each sample and were Rietveld analyzed using the GSAS package. The patterns of samples 1–6 in the $\langle r_A \rangle = 1.223$ Å series were fitted well with the LTO1 model, giving reduced-χ^2 values of 5.9–6.7 which are typical for such data in which the counting errors are small. The mean-squared atomic displacement parameters (*u* factors) were refined as isotropic u_{iso} values for the *A* and Cu cations, but the oxygen parameters were refined anisotropically. Refinement of the off-diagonal u_{ij} terms that are free variables in *Abma* symmetry was not possible as the distortion from tetragonal $I4/mmm$ (HTT) symmetry is small, and so these terms were constrained using the $I4/mmm$ site symmetries. This constrains the principal axes of the real space *u* ellipsoid of mean-squared displacements u_i to the following directions: O(1) $u_1 - [110]_O$, $u_2 - [1\bar{1}0]_O$, and $u_3 - [001]_O$; O(2) $u_1 - [100]_O$, $u_2 - [010]_O$, and $u_3 - [001]_O$ as shown in Fig. 3. Results are shown in Table I and II. Figure 4 shows a typical fit to the D2B data.

The LTO1 structural model gave a poor fit to the 5 K pattern of $\langle r_A \rangle = 1.223$ Å series sample 7 ($\chi^2 = 13.3$). A slightly better fit was obtained with the LTO2 structure ($\chi^2 = 11.1$) but not with an LTT model, which gave an unstable refinement. The best fit was achieved by using a two phase mixture of the LTO1 and LTO2 types. The data for sample 8 were fitted poorly ($\chi^2 > 15$) with single LTO1, LTO2, or LTT phase refinements and so two-phase refinements were performed. The best fit was obtained with a combination of LTO2 and LTT phases. Table III shows the refined parameters for samples 7 and 8.

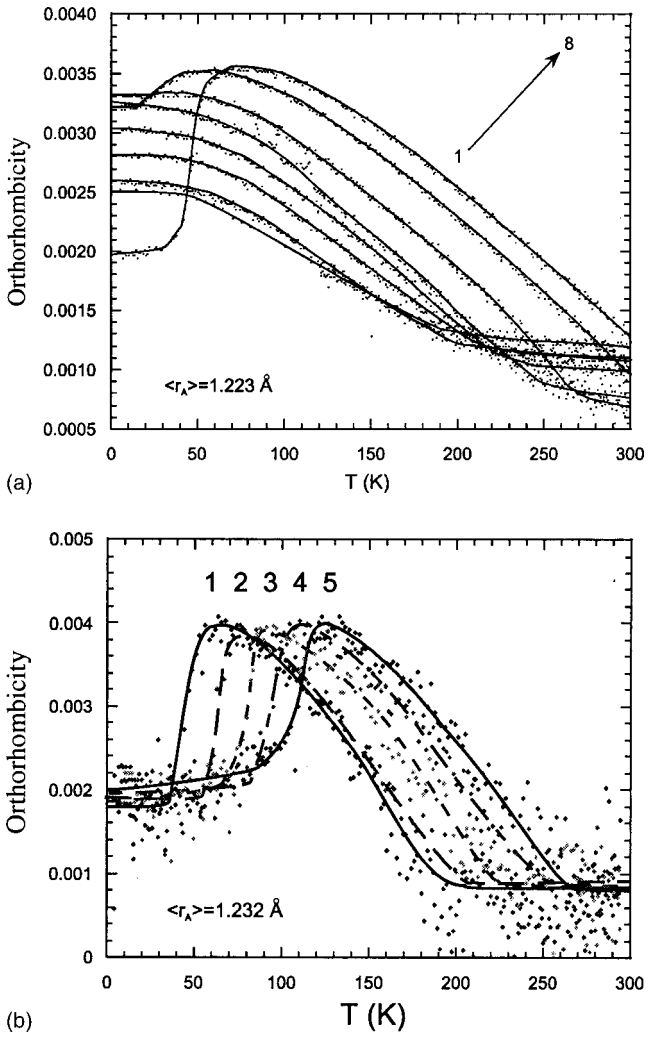

FIG. 1. Orthorhombicity plotted against temperature for (a) the eight $\langle r_A \rangle = 1.223$ Å samples (D20 data), and (b) the five $\langle r_A \rangle = 1.232$ Å samples (D1B data) of $L_{1.85}M_{0.15}CuO_4$ superconductors. The lines are guides for the eye.

The 5 K D2B profiles of the five samples in the $\langle r_A \rangle = 1.232$ Å series were all fitted well by a single LTO2 phase model giving χ^2 values of 5.9–6.8. The LTT model gave significantly poorer fits ($\chi^2 > 8$) and two phase LTO2 and LTT refinements were unstable with the LTT fraction tending to zero. The CuO_2 plane oxygen sites O(1*a*) and O(1*b*) are inequivalent in the LTO2 structure, but their anisotropic displacement parameters were constrained to be equal in the refinements, which were refined with the constraints used in the previous series above. The results are summarized in Tables I and IV.

The refined atomic parameters were used to calculate the Cu-O distances $D_{\text{Cu-O(1)}}$, etc., the tilt angle of the axial Cu-O bonds, θ_a, and the buckling angle of the Cu-O(1)-Cu linkages in the CuO_2 planes, θ_p, as shown in Fig. 3. The r.m.s. (root-mean-squared) fluctuations in the above quantities were also calculated from the corresponding u_i values e.g., the r.m.s. fluctuation in θ_p is $s\theta_p = \tan^{-1}\{\sqrt{u_3}[\text{O}(1)]/D_{\text{Cu-O(1)}}\}$. The quantities showing significant correlations with the *A* cation size variance σ^2 are plotted in Figs. 5–8.

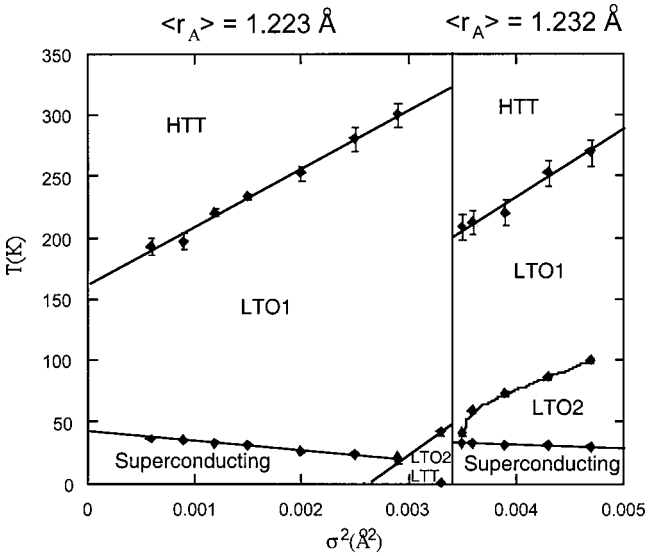

FIG. 2. Structural and superconducting transition temperatures plotted against σ^2 for the $\langle r_A \rangle = 1.223$ and 1.232 Å series of $L_{1.85}M_{0.15}CuO_4$ superconductors.

RESULTS AND DISCUSSION

The neutron-diffraction studies show how the cation size variance σ^2 influences the stability of, and transitions between, the structural phases, and the evolution of the orthorhombic strain and the internal structural parameters. Each of these is described in detail below, followed by phase diagrams for 15% doped A_2CuO_4 which summarize the properties in a useful diagrammatic way.

Structural phase stability and transitions

The results in Table I show that the average cell volume of the A_2CuO_4 materials is constant (to within 0.15%) when

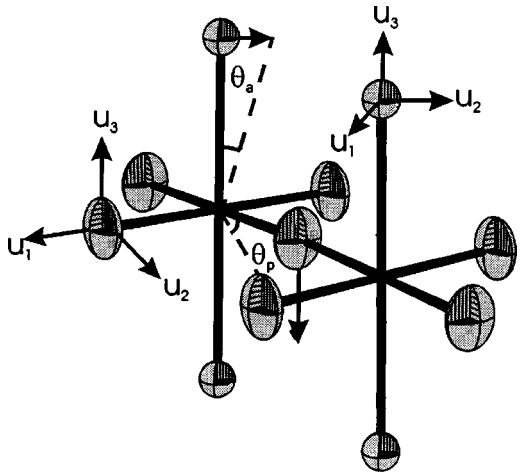

FIG. 3. Directions of the principal axes of the oxygen displacement ellipsoids and definition of the (tilting) θ_a and (buckling) θ_p angles for the CuO_6 octahedra. The tilting is towards $[100]_O$ for the LTO1 structures and $[110]_O$ for the LTO2 and LTT types.

TABLE II. Atomic coordinates, thermal factors, and bond lengths and angles at 5 K for samples 1–6 in the $\langle r_A \rangle = 1.223$ Å series which have the LTO1 structure (space group *Abma*). The atomic positions are: *A* (La, Nd, Ca, Sr, Ba) $[x,0,z]$, Cu [0,0,0], O(1) $[\frac{1}{4},\frac{1}{4},z]$, and O(2) $[x,0,z]$; in the HTT structure the $A{:}x$, O(1):z and O(2):x coordinates are 0.

Sample	1	2	3	4	5	6
$A{:}x$	0.0058(2)	0.0058(2)	0.0062(2)	0.0062(2)	0.0063(2)	0.0065(2)
$A{:}z$	0.360 70(5)	0.360 72(5)	0.360 72(5)	0.360 73(5)	0.360 73(5)	0.360 66(5)
$A{:}u_{iso}$/Å^2	0.0031(2)	0.0031(2)	0.0027(2)	0.0025(1)	0.0024(1)	0.0028(2)
Cu:u_{iso}/Å^2	0.0022(2)	0.0022(2)	0.0021(2)	0.0021(2)	0.0023(2)	0.0027(2)
O(1):z	0.0047(1)	0.0047(1)	0.0052(1)	0.0054(1)	0.0057(1)	0.0059(1)
O(2):x	−0.0216(3)	−0.0224(3)	−0.0240(3)	−0.0252(2)	−0.0264(2)	−0.0275(2)
O(2):z	0.181 96(7)	0.182 14(8)	0.182 16(8)	0.182 30(8)	0.182 33(8)	0.182 63(9)
O(1):u_1/Å^2	0.0017(1)	0.0018(1)	0.0015(1)	0.0016(1)	0.0017(1)	0.0018(1)
O(1):u_2/Å^2	0.0050(3)	0.0052(3)	0.0043(3)	0.0047(3)	0.0049(3)	0.0054(4)
O(1):u_3/Å^2	0.0088(5)	0.0082(5)	0.0094(5)	0.0093(5)	0.0100(6)	0.0117(6)
O(2):u_1/Å^2	0.0103(5)	0.0103(5)	0.0094(5)	0.0106(6)	0.0098(6)	0.0105(6)
O(2):u_2/Å^2	0.0088(4)	0.0098(4)	0.0097(4)	0.0105(4)	0.0117(4)	0.0129(4)
O(2):u_3/Å^2	0.0067(4)	0.0059(4)	0.0058(4)	0.0044(5)	0.0068(4)	0.0079(5)
A-O(1)/Å	2.607(2)/2.663(2)	2.607(1)/2.662(2)	2.604(1)/2.665(1)	2.602(1)/2.668(1)	2.600(1)/2.670(1)	2.599(1)/2.672(1)
A-O(2)/Å	2.363(1)	2.361(1)	2.361(1)	2.358(1)	2.358(1)	2.354(1)
Cu-O(1)/Å	1.887 49(6)	1.887 80(6)	1.888 73(6)	1.889 47(6)	1.890 48(7)	1.890 93(7)
Cu-O(2)/Å	2.4045(11)	2.4060(10)	2.4060(10)	2.4072(11)	2.4076(11)	2.4095(11)
Cu-O(1)-Cu/°	176.2(1)	176.2(1)	175.9(1)	175.7(1)	175.5(1)	175.3(1)
χ^2	5.89	6.64	6.66	6.45	6.64	6.60
R_{WP}/%	4.86	5.01	4.97	4.90	5.03	5.08

σ^2 is varied at fixed doping level and mean *A* cation radius $\langle r_A \rangle$. Furthermore, a positive linear variation of the structural transition temperatures with σ^2 is observed in Fig. 2. This demonstrates that σ^2 is a good experimental approximation to a volume-preserving strain that couples strongly to the order parameter for the structural transitions. Only for the LTO1→LTO2 transition in sample $L1$ of the $\langle r_A \rangle = 1.232$ Å series is a deviation from a linear trend found, and it is difficult to assess whether this results from nonlinear behavior as the transition point decreases towards zero temperature on the basis of one measurement. The linear variation of the structural transition temperatures with σ^2 is of greater magnitude and of opposite sign to the superconducting T_c variations[19] in both series, for $\langle r_A \rangle = 1.223$ Å; $dT_{HTT\rightarrow LTO1}/d\sigma_2 = 48(2)$ kK Å^{-2} whereas dT_c/dÅ$\sigma^2 = -6.8(3)$ kK Å^{-2}; for $\langle r_A \rangle = 1.232$ Å, $dT_{HTT\rightarrow LTO1}/d\sigma^2 = 56(9)$ kK Å^{-2}, and $dT_{LTO1\rightarrow LTO2}/dp = 37(2)$ kK Å^{-2} whereas $dT_c/d\sigma^2 = -3.3(4)$ kK Å^{-2}.

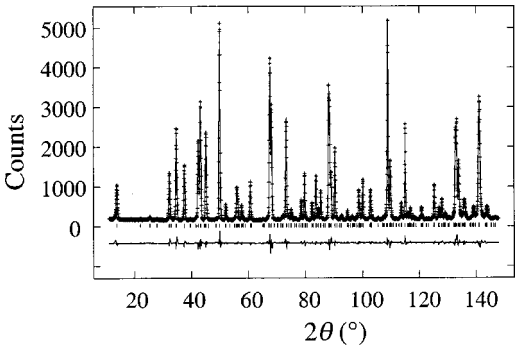

FIG. 4. The Rietveld fit to the D2B neutron-diffraction data for $La_{1.85}Sr_{0.038}Ba_{0.112}CuO_4$ (sample $L1$ of the $\langle r_A \rangle = 1.232$ Å series), showing the observed, calculated, and difference curves.

The structural transitions are known to occur in the sequence HTT→LTO1→LTO2→LTT with decreasing temperature,[11] and the results in Fig. 2 show that the same sequence is followed by increasing σ^2 at constant temperature. In the former case, the sequence is driven by decreasing the thermal entropy which depopulates the phonon modes, but in the latter, the zero-point entropy is increasing. This stabilization may be enthalpic, as increasing σ^2 increases the amplitude for the twists or rotations of the octahedra as described later.

The 5 K structure refinements show that the LTO2 and LTT phases coexist in $\langle r_A \rangle = 1.223$ Å sample 8, but all of the 1.232 Å refinements show no evidence for any LTT phase. This shows that the LTT superstructure is stable only below a critical $\langle r_A \rangle$ value which is between 1.223 and 1.232 Å for 15% doped A_2CuO_4 materials. Comparing these structural data against the previously reported physical measurements on the same samples[19] demonstrates that the presence of the LTT superstructure quenches superconductivity as found in earlier works.[5,7,23] Sample 8 containing 40% LTT and 60% LTO2 phase was not found to be superconducting, whereas all those in the 1.232 Å series which are found to contain only LTO2 at low temperatures within the diffractometer resolution have clear resistive and magnetic superconducting transitions.[19] Electron microscopy has shown that the LTT phase nucleates and grows at the twin boundaries in the orthorhombic phase,[14] so that the two are likely to be intergrown in sample 8. The efficiency with which the LTT dis-

TABLE III. Refined phase fractions, atomic coordinates, thermal factors, and bond lengths and angles at 5 K for samples 7 and 8 in the $\langle r_A \rangle = 1.223$ Å series. The space groups LTO1: *Abma* (see Table I for atomic positions), LTO2: *Pccn* (*A* [*x*,*y*,*z*], Cu [0,0,0], O(1*a*) [$\frac{1}{4},\frac{1}{4},z$], O(1*b*) [$\frac{1}{4},\frac{3}{4},z$], and O(2) [*x*,*y*,*z*]), and LTT: $P4_2/ncm$ (*A* [*x*,*x*,*z*], Cu [0,0,0], O(1*a*) [$\frac{1}{4},\frac{1}{4},z$], O(1*b*) [$\frac{3}{4},\frac{1}{4},0$], and O(2) [*x*,*x*,*z*]) were used.

Sample (type)	7 (LTO1)	7 (LTO2)	8 (LTO2)	8 (LTT)
Phase fractions	0.815(7)	0.185(7)	0.68(1)	0.32(1)
A:*x*	0.0069(2)	0.006(2)	0.0072(5)	0.0043(4)
A:*y*		0.008(1)	0.0062(9)	
A:*z*	0.361 05(9)	0.3594(4)	0.3608(2)	0.3605(2)
$A{:}u_{iso}/\text{Å}^2$	0.0019(3)	0.007(1)	0.0052(6)	−0.0015(8)
$\text{Cu}{:}u_{iso}/\text{Å}^2$	0.0015(3)	0.007(1)	0.0059(6)	−0.0028(9)
O(1*a*):*z*	0.0065(2)	0.005(2)	0.0100(8)	0.0079(7)
O(1*b*):*z*		0.006(2)	0.002(1)	
O(2):*x*	−0.0285(3)	0.019(3)	0.0275(6)	−0.0210(6)
O(2):*y*		0.478(2)	0.488(2)	
O(2):*z*	0.1818(2)	0.3141(6)	0.3182(3)	0.1834(4)
$\text{O}(1a),\text{O}(1b){:}u_1/\text{Å}^2$	0.0016(2)	0.0026(6)	0.0036(8)	−0.005(2)[a]
$\text{O}(1a),\text{O}(1b){:}u_2/\text{Å}^2$	0.0049(5)	0.008(2)	0.011(1)	
$\text{O}(1a),\text{O}(1b){:}u_3/\text{Å}^2$	0.014(1)	0.007(4)	0.022(1)	
$\text{O}(2){:}u_1/\text{Å}^2$	0.0103(7)	0.019(4)	0.015(1)	0.006(1)[a]
$\text{O}(2){:}u_2/\text{Å}^2$	0.0133(6)	0.017(4)	0.019(2)	
$\text{O}(2){:}u_3/\text{Å}^2$	0.0046(9)	0.026(5)	0.011(1)	
A-O(1*a*)/Å	2.592(2)/2.672(2)	2.65(2)/2.64(2)	2.690(8)/2.580(8)	2.686(7)/2.587(7)
A-O(1*b*)/Å		2.69(2)/2.60(2)	2.64(1)/2.62(1)	2.635(2)
A-O(2)/Å	2.368(2)	2.296(9)	2.366(5)	2.340(6)
Cu-O(1*a*)/Å	1.8918(1)	1.8905(8)	1.8945(7)	1.8925(5)
Cu-O(1*b*)/Å		1.891(1)	1.8901(2)	1.889 67(3)
Cu-O(2)/Å	2.3992(2)	2.453(8)	2.399(4)	2.420(5)
Cu-O(1*a*)-Cu/°	174.9(1)	176.4(2)	172.1(6)	173.7(6)
Cu-O(1*b*)-Cu/°		175.4(2)	178.7(8)	180.0
χ^2	5.19		7.06	
R_{WP}/%	4.32		5.05	

[a]Isotropic oxygen thermal factors were refined for the LTT phase.

tortion suppresses superconductivity is remarkable as the structural results for the LTT phase (Table III) differ little from those for the superconducting LTO2 phases in sample 7 or the $\langle r_A \rangle = 1.232$ Å samples in Table IV. Furthermore, the Cu-O-Cu angles for the LTT phase are not more distorted than those in the superconducting LTO2 phases. A possible explanation is that superconductivity is quenched by pinning of the carriers in the LTT regions as charge ordered stripes which extend into the majority LTO2 phase so that the effect is microstructural in origin.

Orthorhombic strain

The orthorhombic strain *o* data in Fig. 1 and Table I reveal systematic trends in the LTO1→HTT and LTO1→LTO2 structural transitions, although it is not clear what critical strain or other structural parameters drive the LTO2→LTT transition. On warming through the high-temperature LTO1→HTT transition, *o* reaches a minimum value o_{HTT}. The true value of the macroscopic orthorhombic strain in the high-temperature phase is zero, however, any additional microscopic strain broadening above the transition is modelled by a finite o_{HTT} in the profile fits. o_{HTT} is limited by the D1B diffractometer resolution of the $\langle r_A \rangle = 1.232$ Å series data in Fig. 1(b), but the instrumental resolution of the D20 $\langle r_A \rangle = 1.223$ Å data is higher and Fig. 1(a) shows that o_{HTT} *decreases* with increasing σ^2, although a lattice microstrain resulting from cation size fluctuations should cause o_{HTT} to *increase* with σ^2. This may be a kinetic effect, resulting from the presence of small metastable domains of untransformed orthorhombic phase above the transition which are annealed out in the critical region around the structural transition more completely as the transition temperature rises and so as σ^2 increases. These observations show that lattice microstrains are also tuned by σ^2.

The data in Fig. 1 also show that the LTO1→LTO2 (+LTT) transition occurs when a critical maximum value of orthorhombic strain, o_c, is reached. With decreasing temperature, all of the $\langle r_A \rangle = 1.232$ Å series in Fig. 1(b) reach the same maximum value of $o_c = 0.004$ and then transform to the LTO2 type which has a constant value of *o* at low temperatures. This is confirmed by the fits to the more highly resolved D2B data which show a remarkably constant $o = 0.0012$ at 5 K (Table I). It is notable that the cell volume also shows no systematic change with σ^2 across the $\langle r_A \rangle$

TABLE IV. Atomic coordinates, thermal factors, and bond lengths and angles at 5 K for the $\langle r_A \rangle = 1.232$ Å samples. The LTO2 model (see Table III) was used for all the fits.

Sample	*L*1	*L*2	*L*3	*L*4	*L*5
A:*x*	0.0060(4)	0.0060(4)	0.0055(5)	0.0057(5)	0.0053(5)
A:*y*	0.0007(8)	0.001(1)	0.0017(9)	0.0021(8)	0.0035(8)
A:*z*	0.360 82(5)	0.360 75(5)	0.360 81(5)	0.360 74(5)	0.360 77(5)
$A{:}u_{iso}/\text{Å}^2$	0.0021(2)	0.0010(2)	0.0021(2)	0.0001(2)	0.0011(2)
$\text{Cu}{:}u_{iso}/\text{Å}^2$	0.0013(2)	0.0005(2)	0.0020(2)	0.0016(2)	0.0012(2)
O(1*a*):*z*	0.0075(3)	0.0075(3)	0.0079(3)	0.0080(3)	0.0084(3)
O(1*b*):*z*	−0.001(1)	−0.001(1)	0.0001(9)	0.0013(9)	0.000(1)
O(2):*x*	0.0213(6)	0.0215(6)	0.0213(6)	0.0226(7)	0.0229(7)
O(2):*y*	0.490(1)	0.491(2)	0.490(1)	0.487(1)	0.485(1)
O(2):*z*	0.318 21(8)	0.318 11(8)	0.318 18(8)	0.318 01(9)	0.318 06(9)
$\text{O}(1a),\text{O}(1b){:}u_1/\text{Å}^2$	0.0016(1)	0.0012(1)	0.0018(1)	0.0016(1)	0.0014(1)
$\text{O}(1a),\text{O}(1b){:}u_2/\text{Å}^2$	0.0049(4)	0.0036(4)	0.0055(4)	0.0049(4)	0.0042(4)
$\text{O}(1a),\text{O}(1b){:}u_3/\text{Å}^2$	0.0102(6)	0.0093(6)	0.0116(7)	0.0114(7)	0.0113(7)
$\text{O}(2){:}u_1/\text{Å}^2$	0.010(1)	0.009(1)	0.011(1)	0.010(1)	0.011(1)
$\text{O}(2){:}u_2/\text{Å}^2$	0.013(1)	0.014(1)	0.016(1)	0.016(1)	0.014(1)
$\text{O}(2){:}u_3/\text{Å}^2$	0.0061(4)	0.0065(5)	0.0059(5)	0.0061(5)	0.0054(5)
A-O(1*a*)/Å	2.590(1) /2.691(3)	2.590(3) /2.692(3)	2.588(3) /2.694(3)	2.589(3) /2.694(3)	2.587(3) /2.694(3)
A-O(1*b*)/Å	2.630(9) /2.649(9)	2.63(1) /2.649(9)	2.628(9) /2.694(3)	2.618(9) /2.661(9)	2.63(1) /2.64(1)
A-O(2)/Å	2.374(1)	2.372(1)	2.374(1)	2.370(2)	2.371(1)
Cu-O(1*a*)/Å	1.8926(2)	1.8924(2)	1.8931(2)	1.8935(2)	1.8940(2)
Cu-O(1*b*)/Å	1.890 03(5)	1.889 82(5)	1.890 27(2)	1.8906(1)	1.890 77(2)
Cu-O(2)/Å	2.409(1)	2.410(1)	2.409(1)	2.411(1)	2.410(1)
Cu-O(1*a*)-Cu/°	174.0(2)	174.0(2)	173.7(2)	173.6(2)	173.3(2)
Cu-O(1*b*)-Cu/°	179.5(6)	179.6(6)	179.907(1)	178.9(7)	180.0(4)
χ^2	5.91	6.80	6.19	6.79	6.34
$R_{WP}/\%$	4.87	5.19	5.04	5.27	5.01

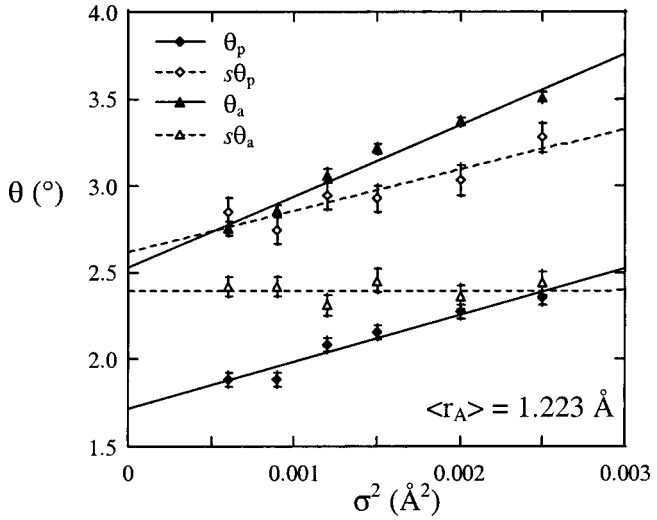

FIG. 5. The mean buckling (θ_p) and tilting (θ_a) angles and their r.m.s. deviations ($s\theta_p$ and $s\theta_a$) plotted against σ^2 for the $\langle r_A \rangle = 1.223$ Å series, with linear fits.

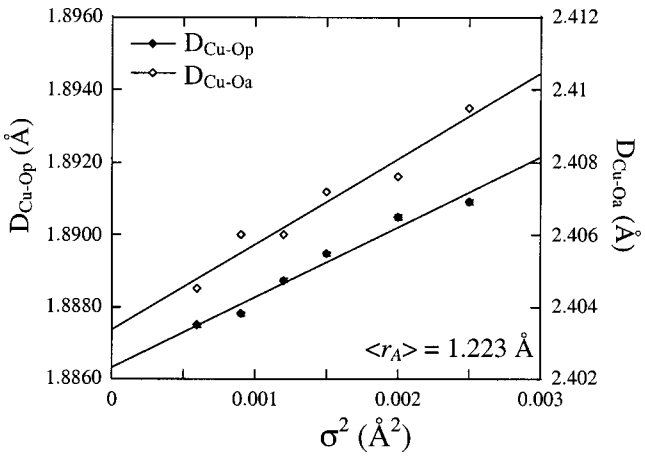

FIG. 6. The mean in-plane ($D_{\text{Cu-O}p}$) and apical ($D_{\text{Cu-O}a}$) distances plotted against σ^2 for the $\langle r_A \rangle = 1.223$ Å series, with linear fits.

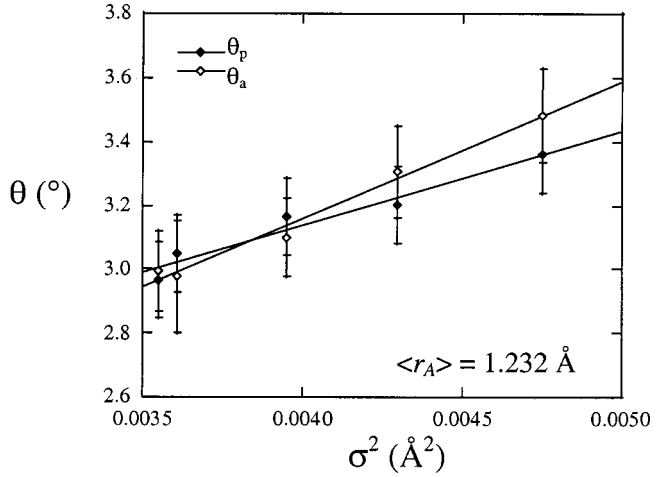

FIG. 7. The mean buckling (θ_p) and tilting (θ_a) angles plotted against σ^2 for the $\langle r_A \rangle = 1.232$ Å series. θ_p is calculated for O(1*a*) as O(1*b*) causes no significant buckling of the CuO_2 planes (see Table IV).

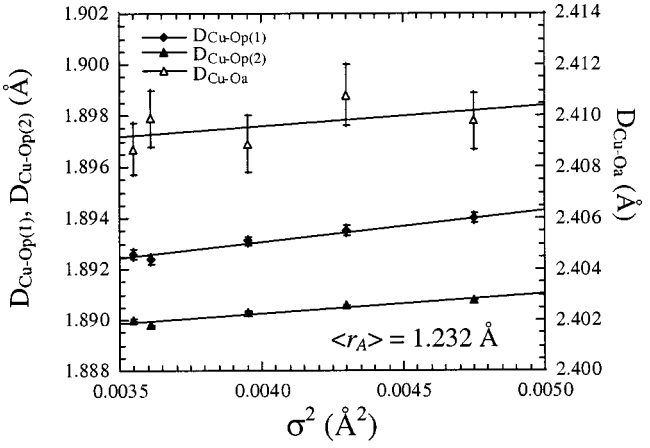

FIG. 8. The mean in-plane [$D_{\text{Cu-O}p}(1)$ and $D_{\text{Cu-O}p}(2)$] and apical ($D_{\text{Cu-O}a}$) distances plotted against σ^2 for the $\langle r_A \rangle = 1.223$ Å series, with linear fits.

$=1.232$ Å series although the cell parameters themselves show systematic changes (*a* and *b* increase while *c* decreases). This demonstrates that σ^2 describes a strain that is both volume- and orthorhombicity-preserving in the LTO2 structure.

In the $\langle r_A \rangle = 1.223$ Å D20 data [Fig. 1(a)], the saturated orthorhombic strain in the LTO1 phase increases as $T_{\text{LTO1}\rightarrow\text{HTT}}$ increases. Samples 1–6 remain LTO1 type down to the lowest observed temperatures, but samples 7 and 8 exceed o_c and transform to the other structure types. Sample 7 partially transforms to LTO2, whereas sample 8 reaches o_c at a higher temperature and transforms completely to LTO2 and LTT. The 5 K D2B refinements (Table I) show that the LTO1-type samples 1–6 have *o* increasing to 0.0066 and the LTO1 component in sample 7 has $o_c = 0.0069$ whereas the LTO2 component has $o = 0.0026$. Comparison of the 5 K cell data in Table I shows that *a* and *b* increase and *c* decreases with σ^2 for the LTO1 phases as found for the LTO2 types above. However, the cell volume increases slightly and the saturated orthorhombic strain increases strongly with σ^2 in the LTO1 structure type.

Internal structure

The refinements of the LTO1 type samples 1–6 in the $\langle r_A \rangle = 1.223$ Å series and the LTO2-type $\langle r_A \rangle = 1.232$ Å samples enable the evolution of internal structural parameters with σ^2 to be studied. To estimate changes in local structural disorder with σ^2, r.m.s. deviations of the oxygen atoms about their mean positions have been calculated from the principal values of the *u* tensor. Both thermal motion and static fluctuations contribute to *u* and the two effects cannot be separated rigorously from diffraction measurements. However, it is reasonable to assume that the thermal contribution is small and approximately constant at 5 K, so that changes in *u* reflect the increasing disorder due to σ^2.

As described above, the saturated orthorhombic strain in the LTO1-type $\langle r_A \rangle = 1.223$ Å samples (Table I) increases as σ^2 increases, and there is a slight decrease in the *c* cell constant. There is a corresponding increase in the deviation of the atomic coordinates (Table II) from those of the ideal HTT structure, which leads to increases in the buckling angle of the Cu-O-Cu planes (θ_p) and the tilt angle of the apical oxygen from the *c* axis (θ_a) as shown in Fig. 5. Surprisingly, the r.m.s. deviations $s\theta$ in these angles have rather different σ^2-dependences. $s\theta_p$ exceeds θ_p by 0.8° and shows the same, linear, rate of increase with σ^2, whereas $s\theta_a$ is less than θ_a and shows no significant change with σ^2. This demonstrates that the cation size variance σ^2 creates static fluctuations of the Cu-O-Cu buckling angle, but not in the apical angle for which vibrational fluctuations are limiting. The in-plane Cu-O(1) and apical Cu-O(2) bond lengths also increase with σ^2 (Fig. 6), but the r.m.s. deviations in these distances show no significant variation with σ^2 and are not plotted.

The $\langle r_A \rangle = 1.232$ Å samples have LTO2 symmetry at 5 K. The orthorhombicity and cell volume are very constant with σ^2 but the *a* and *b* cell parameters increase slightly and *c* decreases across the series (Table I). One of the Cu-O-Cu bond angles remains linear while the other increasingly bends as σ^2 increases (plotted as θ_p in Fig. 7) and the in-plane Cu-O bond lengths increase accordingly to accommodate this distortion (Fig. 8). The statistical errors in the r.m.s. deviations in the distances and angles are too great to allow any significant trends with σ^2 to be observed, but the $s\theta_p$ and $s\theta_a$ fluctuations of ~3° are comparable to the mean values in Fig. 7. Hence the refinements of the $\langle r_A \rangle = 1.232$ Å samples again demonstrate that the suppression of T_c in these series correlates with increasing mean tilting and buckling angles, but angular fluctuations comparable to the mean distortion angles are also present although their σ^2 variation is not determined.

The 5 K structure refinements of two series of isovariant, isoelectronic $L_{1.85}M_{0.15}CuO_4$ compositions with different superstructures show that increasing the cation size variance σ^2 leads to larger tilts of the CuO_6 octahedra and Cu-O-Cu buckling angles, which are known to suppress T_c.[2,24] To compare the effects of changing the apical and buckling

angles $\theta_{(a\ or\ p)}$ on the superconducting transition temperature T_c in the two series, the slopes $dT_c/d\theta$ have been calculated as

$$dT_c/d\theta=(dT_c/d\sigma^2)/(d\theta/d\sigma^2),$$

giving $dT_c/d\theta_p=-24(3)$ and $dT_c/d\theta_a=-16(1)$ K deg^{-1} for the $\langle r_A\rangle=1.223$ Å LTO1 samples and $dT_c/d\theta_p=-11(2)$ and $dT_c/d\theta_a=-8(1)$ K deg^{-1} for the LTO2-type $\langle r_A\rangle=1.232$ Å series. It is notable that the values for the former series are twice those for the latter. This may arise because in the LTO1-type structure, the Cu-O-Cu bridges in the $[110]_O$ and $[1\bar{1}0]_O$ directions both bend with angle θ_p, whereas in the LTO2 type only the $[110]_O$ Cu-O-Cu angle bends as θ_p while the other angle remains approximately constant at ~180°.

The coincidence of $dT_c/d\theta_p$ per Cu-O-Cu bridge in both the LTO1 and LTO2 series emphasizes the importance of the buckling angle for superconductivity, in agreement with other studies which have shown that T_c decreases as the buckling angle θ_p increases.[2,24] This is written as $(\partial T_c/\partial\theta_p)_{x,\langle r_A\rangle}=-12$ K deg^{-1} to emphasize that it measures the change of T_c with mean buckling angle by changing σ^2 at constant $\langle r_A\rangle$ and doping level x. This can be compared against the value of $(\partial T_c/\partial\theta_p)_{x,\sigma^2}=-4$ K deg^{-1} per Cu-O-Cu bridge derived from a study of the LTO1-type $La_{1.85-y}Nd_yCa_{0.15}CuO_4$ ($0<y<1$) series[25] in which the A cation size disorder is small and approximately constant ($\sigma^2<0.0007$ Å^2) and the structural changes are driven by decreasing $\langle r_A\rangle$. The additional contribution to $(\partial T_c/\partial\theta_p)_{x,\langle r_A\rangle}$ compared to $(\partial T_c/\partial\theta_p)_{x,\sigma^2}$ is attributed to the increase in the static fluctuations in the buckling angle $s\theta_p$ with σ^2 as shown in Fig. 5. The rate of suppression of T_c by the r.m.s. fluctuations $s\theta_p$ is thus estimated to be ~2 times the rate of change with the mean θ_p angle. This shows that superconductivity in the $L_{1.85}M_{0.15}CuO_4$ system is more sensitive to structural fluctuations, which may act as pinning sites for charge ordered stripe domains,[10,26] than to changes in average structure that modify the electronic density of states,[2] although the two effects are of comparable magnitude.

Phase diagrams

Recent work on $(L_{1-x}M_x)MnO_3$ perovskites has shown that a good first approximation phase diagram can be constructed by plotting the temperature variation of properties at a constant doping level x on the $\langle r_A\rangle$-σ^2 plane.[27] This contains all $(L_{1-x}M_x)$ combinations for any number of L^{3+} and M^{2+} cations at a given x value, all of which lie within a bounded region known as the ''chemical window.'' The chemical window for the $L_{1.85}M_{0.15}CuO_4$ system (for L^{3+} = La-Eu; M^{2+} = Ca, Sr, Ba) is shown in Fig. 9(a). The important boundary is the high $\langle r_A\rangle$ and low σ^2 frontier defined by the $La_{1.85}Ca_{0.15}$, $La_{1.85}Sr_{0.15}$, and $La_{1.85}Ba_{0.15}$ compositions, beyond which no $L_{1.85}M_{0.15}CuO_4$ materials exist. Substitution of other cations such as smaller L^{3+} produces samples with lower $\langle r_A\rangle$ and higher σ^2. This leads to a change from La_2CuO_4-type (T) to Nd_2CuO_4-type (T') phases below $\langle r_A\rangle\approx1.20$ Å.[28]

The structural phase transition temperatures have been used to construct the structural phase diagram in Fig. 9(b). This shows approximate isotherms for the HTT→LTO1 and LTO1→(LTO2 and LTT) transitions. The former transition is described by linear isotherms, but the latter shows a nonlinear boundary. All four structure types are stable at $T=0$ in different regions of the phase diagram, although these do not all lie within the chemical window. The HTT structure is the ground state only at higher $\langle r_A\rangle$ and lower σ^2 values than are observable, whereas LTO1 is stable around the low σ^2 edge of the chemical window. The LTO2 and LTT types are found at higher σ^2; the LTT type appears to be stabilized at lower $\langle r_A\rangle$ than LTO2.

The electronic phase diagram for the $L_{1.85}M_{0.15}CuO_4$ system in Fig. 9(c) has been constructed from the T_c values for our samples[19] and other reported $L_{1.85}M_{0.15}CuO_4$ materials.[29–33] Two features of this distribution are striking. Only five compositions with $0<T_c<20$ K have been reported in comparison to the 19 samples with $20<T_c<40$ K, from which the isotherms have been derived. These are generally consistent with the data, except in the region close to the $La_{1.85}Ca_{0.15}$ composition, where high pressures are needed to ensure sample homogeneity.[34] The second surprising feature is that the isotherms show a pronounced deformation in comparison to the smooth curves that would be expected by analogy with previous work on the $(L_{1-x}M_x)MnO_3$ perovskites.[28] The position of the bulge corresponds to the region at which the LTT structure is stable showing that this instability suppresses superconductivity in a large part of the chemical window. Good $L_{1.85}M_{0.15}CuO_4$ superconductors are only observed close to the $La_{1.85}Ca_{0.15}$-$La_{1.85}Sr_{0.15}$-$La_{1.85}Ba_{0.15}$ boundary of the window (and T_c would continue to rise if materials could be made beyond this boundary). Few $L_{1.85}M_{0.15}CuO_4$ materials with a finite T_c below 20 K have been reported, as the LTT and superconducting regions meet near the $T_c=20$ K isotherm.

CONCLUSIONS

The results presented here demonstrate that the structural properties of $L_{1-x}M_xCuO_4$ materials, in addition to their previously reported superconducting parameters,[19] are usefully described by the doping level x, the mean A site cation radius $\langle r_A\rangle$ (equivalent to the traditional perovskite tolerance factor) and the variance in the A cation radii σ^2. It was originally assumed that changing only $\langle r_A\rangle$ or σ^2 would change only the average structure or local structural fluctuations, respectively. However, the present study shows that the average structure of $L_{1.85}M_{0.15}CuO_4$ materials also changes systematically with σ^2, as local strains are in part accommodated through coherent tilting of the octahedra.

The A cation size variance σ^2 couples strongly to the orthorhombic macrostrain resulting in a strong, positive linear correlation between the structural transition temperatures and σ^2. This in turn leads to increasing distortions of the

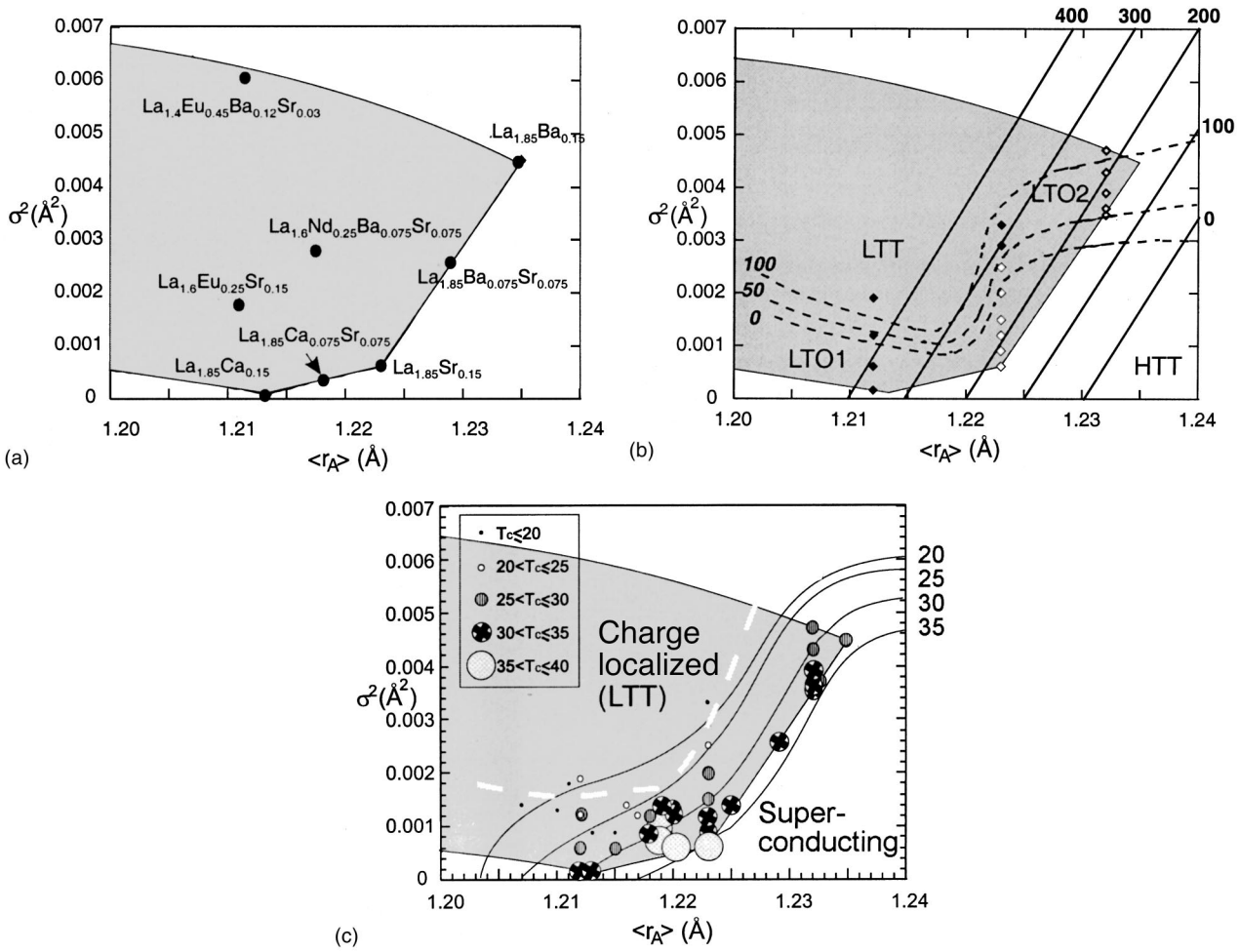

FIG. 9. Phase diagrams for the $L_{1.85}M_{0.15}CuO_4$ system projected onto the $\langle r_A\rangle$-σ^2 plane. (a) The chemical window (shaded) contains all the possible compositions for L=La-Eu and M=Ba, Sr, and Ca combinations; the positions of some cation compositions are marked. (b) Variation of superstructure types with approximate isotherms for the HTT→LTO1 transition [full lines; temperatures (K) in upright text] and the LTO1→(LTO2 and LTT) transition (broken lines, temperatures in italics). Results are taken from this and previous studies (Refs. 19 and 33), open/closed symbols have HTT/LTO1 symmetry at room temperature. The phase labels show the region where each is the stable $T=0$ phase. (c) Electronic phase diagram showing T_c values and isotherms (K). The approximate boundary of the nonsuperconducting, charge localized region is taken from the LTT region in (b). The continuations of the isotherms outside the chemical window are hypothetical as no materials exist there.

average crystal structure, in particular the increased bending of the in-plane Cu-O-Cu linkages, which shows the same rate of suppression of superconductivity per distorted Cu-O-Cu bridge in the LTO1- and LTO2-type structures. However, an increase in the r.m.s. static fluctuations of the in-plane buckling angle with σ^2 is also evidenced in the LTO1 samples and these suppress superconductivity at twice the rate of suppression by the mean angle. This supports the original notion that the dominant effect of σ^2 is to create local structural fluctuations that encourage carrier localization, although changes in the average structure that will alter the electronic density of states are also found to be significant. A similar conclusion was reached by neutron-diffraction studies of $L_{0.7}M_{0.3}MnO_3$ perovskites which revealed small changes in the average structure but a large increase in local structural fluctuations with σ^2.[35,36]

Another use of this parametrization is to construct good, first approximation, phase diagrams using x, $\langle r_A\rangle$, and σ^2. These show the chemical window that is available at any given x due to the range of cation sizes available, and enable the temperature dependence of structural and electronic properties to be displayed. We find that the distribution of superconducting critical temperatures contains a significant deformation due to the presence of the LTT structural instability which suppresses superconductivity across a large part of the $x=0.15$ window.

ACKNOWLEDGMENTS

We thank Dr. A. Hewat for assistance in collecting neutron-diffraction data at the ILL and EPSRC for the provision of neutron facilities and financial support for J.A.M.

[1] J. B. Torrance, A. Bezinge, A. I. Nazzal, T. C. Huang, S. S. P. Parkin, D. T. Keane, S. J. Laplaca, P. M. Horn, and G. A. Held, Phys. Rev. B **40**, 8872 (1996).
[2] B. Dabrowski, Z. Wang, K. Rogachi, J. D. Jorgensen, R. L. Hitterman, J. L. Wagner, B. A. Hunter, P. G. Radaelli, and D. G. Hinks, Phys. Rev. Lett. **76**, 1348 (1996).
[3] D. C. Johnston, S. K. Sinha, A. J. Jacobson, and J. M. Newsam, Physica C **153-155**, 572 (1988).
[4] M. Onoda, S. Shamoto, M. Sato, and S. Hosoya, Jpn. J. Appl. Phys., Part 2 **26**, 363 (1987).
[5] J. D. Axe, A. H. Moudden, D. Hohlwein, D. E. Cox, K. M. Mohanty, A. R. Moodenbaugh, and Y. W. Xu, Phys. Rev. Lett. **62**, 2751 (1989).
[6] M. K. Crawford, R. L. Harlow, E. M. McCarron, D. E. Cox, and Q. Huang, Physica C **235-240**, 170 (1994).
[7] D. Haskel, E. A. Stern, F. Dogan, and A. R. Moodenbaugh, J. Synchrotron Radiat. **6**, 755 (1999).
[8] Y. Koike, S. Takeuchi, H. Sato, Y. Hama, M. Kato, Y. Ono, and S. Katano, J. Low Temp. Phys. **105**, 317 (1996).
[9] K. Yoshida, F. Nakamura, Y. Tanaka, Y. Maeno, and T. Fujita, Physica C **230**, 371 (1994).
[10] J. M. Tranquada, B. J. Sternlieb, J. D. Axe, Y. Nakamura, and S. Uchida, Nature (London) **375**, 561 (1995).
[11] M. K. Crawford, R. L. Harlow, E. M. McCarron, W. E. Farneth, J. D. Axe, H. Chou, and Q. Huang, Phys. Rev. B **44**, 7749 (1991).
[12] D. Haskel, E. A. Stern, D. G. Hinks, A. W. Mitchell, J. D. Jorgensen, and J. I. Budnick, Phys. Rev. B **76**, 439 (1996).
[13] D. Haskel, E. A. Stern, D. G. Hinks, A. W. Mitchell, and J. D. Jorgensen, Phys. Rev. B **56**, 521 (1997).
[14] Y. Zhu, A. R. Moodenbaugh, Z. X. Cai, J. Tafto, M. Suenaga, and D. O. Welch, Phys. Rev. Lett. **73**, 3026 (1994).
[15] C. H. Chen, S.-W. Cheong, D. J. Werder, and H. Takagi, Physica C **206**, 183 (1993).
[16] S. J. L. Billinge, G. H. Kwei, and H. Takagi, Phys. Rev. Lett. **72**, 2282 (1994).
[17] D. Haskel, E. A. Stern, F. Dogan, and A. R. Moodenbaugh, Phys. Rev. B **61**, 7055 (2000).
[18] J. P. Attfield, A. L. Kharlanov, and J. A. McAllister, Nature (London) **394**, 157 (1998).
[19] J. A. McAllister and J. P. Attfield, Phys. Rev. Lett. **83**, 3289 (1999).
[20] Ionic radii for nine-coordinate A-site cations are taken from R. D. Shannon, Acta Crystallogr., Sect. A: Cryst. Phys., Diffr., Theor. Gen. Crystallogr. **32**, 751 (1976).
[21] J. Rodriguez-Carvajal, FULLPROF Program, Version 3.5 d, 1998.
[22] A. C. Larson and R. B. Von Dreele, Los Alamos National Laboratory Report No. LA-UR-86-748 1987 (unpublished).
[23] Y. Koyama, Y. Wakabayashi, K. Ito, and Y. Inoue, Phys. Rev. B **51**, 9045 (1995).
[24] B. Büchner, M. Breuer, A. Freimuth, and A. P. Kampf, Phys. Rev. Lett. **73**, 1841 (1994).
[25] A T_c suppression of 16 K for an increase of 4.5° in $2\theta_p$ for the two Cu-O-Cu bridges is shown in Fig. 3 of Ref. 2.
[26] E. S. Bozin, S. J. L. Billinge, G. H. Kwei, and H. Takagi, Phys. Rev. B **59**, 4445 (1999).
[27] L. M. Rodriguez-Martinez and J. P. Attfield, Phys. Rev. B **63**, 024424 (2001).
[28] J. A. McAllister, S. Davies, and J. P. Attfield, J. Solid State Chem. **155**, 138 (2000).
[29] K. Oh-Ishi and Y. Syono, J. Solid State Chem. **95**, 136 (1991).
[30] I. Felner, Solid State Commun. **62**, 791 (1987).
[31] J. M. Tarascon, L. H. Greene, W. R. McKinnon, and G. W. Hull, Solid State Commun. **63**, 499 (1987).
[32] Y. Maeno, N. Kakehi, Y. Tanaka, T. Tomita, F. Nakamura, and T. Fujita, in *Proceedings of the Conference on Lattice Effects in High-T_c Superconductors, Sante Fe, New Mexico*, edited by Y. Bar-Yam, T. Egami, J. Mustre-de-Leon, and A. R. Bishop (World Scientific, Singapore, 1992), pp. 542–547.
[33] B. Büchner, M. Braden, M. Cramm, W. Schlabitz, W. Schnelle, O. Hoffels, W. Braunisch, R. Muller, G. Heger, and D. Wohlleben, Physica C **185-189**, 903 (1991).
[34] B. Dabrowski, Z. Wang, J. D. Jorgensen, R. L. Hitterman, J. L. Wagner, B. A. Hunter, and D. G. Hinks, Physica C **217**, 455 (1993).
[35] L. M. Rodríguez-Martínez and J. P. Attfield, Phys. Rev. B **58**, 2426 (1998).
[36] L. M. Rodríguez-Martínez and J. P. Attfield, Chem. Mater. **11**, 1504 (1999).